Indian Journal of Chemical Technology
Vol. 28, September, 2021 pp. 556-563

Electrocatalytic performance of the cobalt oxide nanoparticles decorated graphene oxide over the detection of folic acid

Boopathy Gopal [1], Keerthi Murugan[2] & Shen-Ming Chen [2,*]

[1]Department of chemistry, college of engineering, Guindy, Anna University, Chennai 600 025, Tamilnadu, India.

[2]Department of Chemical Engineering and Biotechnology, National Taipei University of Technology, No.1, Section 3, Chung-Hsiao East Road, Taipei 106, Taiwan

E-mail: smchen1957@gmail.com, smchen78@ms15.hinet.net

Received 13 February 2021; accepted 01 September 2021

Herein, we Design and synthesis of a composite material consisting of cobalt oxide anchored on graphene oxide (Co_3O_4@GO) as an electrode modifier, and their application to the detection of folic acid (FA) has been investigated. The integration of Co_3O_4 and GO is by hydrothermal assisted synthesis route. The morphology and crystalline structure of the Co_3O_4@GO has been well analyzed by XRD, XPS, FESEM, HR-TEM, and EDX analysis. The electrochemical test of the Co_3O_4@GO modified electrode shows an interesting electrochemical performance for the selective determination of FA with a broad concertation range of 0.1-4000 µM and a lower detection limit (LOD) of 0.024 µM. The enhancement in the catalytic activity of Co_3O_4@GO can be achieved by the synergistic effect of $Co_3O_4$and GO, high electron transportation, and unique spherical structure of Co_3O_4@GO. The newly developed Co_3O_4@GO sensor also displays excellent sensitivity of 47.23 $\mu A \mu M^{-1}$ cm^{-2}. Finally, this Co_3O_4@GO sensor is demonstrated for the detection of FA in the human urine sample with excellent recovery.

Keywords: Cobalt oxide, Electrochemical detection, Folic acid, GO, Modified electrode

Folic acid (Vitamin B9, FA) is a water soluble vitamin which is asignificant one-carbon donor for the synthesis of thymidine and purines (critical components of nucleic acids) and indirectly, for the synthesis of proteins and lipids through the S-adenosyl ethionine methylation of DNA[1]. Folic acid deficiency in animals is the main cause of series of diseases, including fetal neural tube defects, gigantocytic anemia, cardiovascular disease, mental devolution, heart attack, leucopoenia, congenital malformation and cancers[2]. The amount of FA is related to the dealings of hypertension, hypercholesterolemia, hyper homocysteinemic coronary artery disease, depression, mammary tumor etc. Therefore, a precise substratum has to be laid for the early detection of such diseases by quantifying FA in the diagnosis procedure. For this very purpose, development of selective and sensitive methods is to be analyzed while decreasing the proximities of detection[2,3]. The established methods like HPLC and chromatographic techniques have become costlier and less accurate. Moreover, these analytical methods are required luxurious instrumentation, time-consuming, and large scale sample preparation. At the same time, electrochemical methods offer high sensitivity, selectivity, rapid detection in low concentration[3-7].

Graphene oxide (GO) has accomplished great growing interest on developing new electrocatalyst due to its unique electronic structure and π conjugation between the GO layers[4-7]. It has been exhibited photocatalytic[8], electrocatalytic, and heterogeneous catalytic activities and applied to many fields such as water splitting, energy storage and conversion, organic catalysis, and pollution control[9]. In addition, carbon materialsare environmentally-friendly, abundant and inexpensive and excellent light absorption characteristics[10-12]. The catalyst which having hybrid electronic structure is one of the promising material for electrochemical sensor[13-16]. In this view, the an efficient electrocatalyst developed by modifying the electronic structure of GO with appropriate Nanosized metal oxide[17-18]. Meanwhile, GO act as a good substrate to develop hetero-structured electrochemical sensing materials due to its providing anchoring sites to attach owing to its two-dimensional conjugation structure and enhance the electrocatalytic activity[19-21]. The cobalt oxide (Co_3O_4)nanoparticles extensively studied in various

field such as in gas sensors, supercapacitors, solar-energy absorbers, rechargeable lithium-ion battery and electrochemical sensor materials[22-24]. The outstanding performances of Co_3O_4 in such applications, due to its inherent electronic, magnetic, optical, and catalytic properties depends on its crystalline and surface features[25-28]. The crystalline structure of Co_3O_4adopted normal spinel structure based on close packing arrangement of oxide ions, in which Co(II) ions reside in the tetrahedral 8a sites and Co(III) ions reside in the octahedral 16d site[17,29,30]. The electrochemical performance enhanced by altering the inter junction interface of electrochemical nanomaterials by doping the suitable catalyst. Due to the excellent inherent catalytic activity, Co_3O_4 have been also used to modify the GO electronic structure and enhance the electrocatalytic activity. In this study, the conductivity of GO altered with Co_3O_4. It is therefore expected that Co_3O_4@GO can be a favorable catalyst for the electrochemical oxidation of FA.

Experimental Section

Chemicals and Reagents

Cobalt chloride ($CoCl_2.6H_2O$), Sodium hydroxide (NaOH), ascorbic acid ($C_6H_8O_6$), sodium phosphate dibasic (Na_2HPO_4), sodium phosphate monobasic (NaH_2PO_4), hydrochloric acid (HCl, 36.5–38.0 %), sodium hydroxide (NaOH, ≥ 98.0%), folic acid were all purchased from Sigma-Aldrich and used directly as received. The human urine samples were obtained from Chang Gung University (CGU) and the experimental law and protocol was carried out according to the committee of CGU, Taiwan. Double distilled (DD) water and ethanol were used throughout the experiment for washing and solution preparation. 0.1 M of phosphate buffer (PB) was used for the entire electrochemical experiment. PB was prepared by mixing Na_2HPO_4 and NaH_2PO_4 in DD water and their *p*H was adjusted using NaOH, and HCl were used. All chemicals used in these experiments were standard analytical grade.

Instrumentations

The crystallinity of the samples was analyzed by X-ray diffraction (XRD) diffractometer XPERT-PRO (PAN analytical B.V. The Netherlands) with Cu Kα radiation (k = 1.54 Å). The elemental composition and valence state of the Co_3O_4@GOwere scrutinized by X-ray photoelectron spectroscopy (XPS, Thermo ESCALAB 250 instrument). The morphological characterization of the materials studied by the field emission scanning electron microscopy (FESEM, Hitachi S-3000 H) and high resolution-transmission electron microscopy (HR-TEM) H-7600, Hitachi, (Japan). The chemical proportion was assessed through an energy-dispersive X-ray (EDX) affiliated with HR-TEM. The electrochemical characterization of the sensor was examined through electrochemical techniques using electrochemical impedance spectroscopy (EIS)Xpot ZAHNER-elektrik instrument, and electrochemical workstation such as cyclic voltammetry (CV, CHI 1205C), CH Instruments Company, U.S.A. The three-electrode system was used in this experiment was a glassy carbon electrode (GCE) as the working electrode (working area = 0.071 cm^2), Ag/AgCl (saturated KCl) as the reference electrode, and a platinum wire as the counter electrode.

Preparation of Co_3O_4

The Co_3O_4 was prepared according to the previousreport with some modification[31].In the process of the, $CoCl_2.6H_2O$ (0.25 M) and NaOH (1 M) were dissolved in 50 mL of DDwater. After that, the above solution mixture stirred to get the homogeneous formation up to 30 minutes and poured into a autoclave for hydrothermal reaction at 120˚C for 5 h. The obtained $Co_3O_4$was collected and washed several times with DD water and ethanol to eliminate any alkaline salt existent in the above residue and then dehydrated using air oven 60˚for 12 hours. The subsequent formation of Co_3O_4 was collected and calcinated for 1 h at 350˚C in a muffle furnace.

Synthesis of the Co_3O_4 @GO

Graphene oxide was prepared by modified hummer's method. 10 mg each of GO and Co_3O_4nanoparticles were suspended in water and stirred for 15 minutes. The suspension was ultra-sonicated for 30 minutes to enable interfacial self-assembly between the GO and Co_3O_4nanoparticles to form Co_3O_4@GO.

Fabrication of Co_3O_4 @GO/GCE modified electrode

The synthesized Co_3O_4@GO powder 2 mg was dispersed in DD water (1 mL) via ultrasonic treatment for 20 min to get homogeneouss slurry. For control studies, Co_3O_4 and GO was prepared separately. Before each experiment, the bare GCE was cleaned using alumina powder on a polishing pad and then ultra-sonicated in a mixture of DD water and ethanol (1:1). Then, 6.0 μL of Co_3O_4@GOwas coated on the

pretreated GCE with a micropipette and then dried at 37˚C.

Results and Discussion

Structural characterization of Co_3O_4 @GO

The crystalline natures of the synthesized GO,Co_3O_4 and Co_3O_4@GO were investigated by XRD shown in Fig. 1A. In the XRD pattern of GO, the characteristic diffraction peak of (002) plane observed at 10˚. In the XRD pattern of Co_3O_4, the characteristics peaks observed at 33˚, 46˚, 65˚, 79˚ corresponding to (220), (400), (440) and (533) crystal planes (JCPDSNo.42-1467)[33]. Interestingly, the XRD patterns of the nanocomposite to be identical of Co_3O_4 and characteristic peaks of disappeared due to the strong interaction of Co_3O_4 NPs and GO.

The FT-IR spectrum was collected to understand the chemical bonding of the Co_3O_4 and GO (Fig. 1B). The two peaks at 3405 cm^{-1} and 1420 cm^{-1} were observed in the GO spectrum due to the vibration and deformation of O-H bond. The another two peaks at 1070 cm^{-1} and 1631 cm^{-1} is due to C-O stretching, C=C stretching vibrations from unoxidized graphitic domains, respectively[34]. The Co_3O_4spectrum shows two new and weak peaks at 675 and 490 cm^{-1} responsible for the typical stretching vibration of Co (II) O and Co(III) O[35]. The intensity of C=O stretching vibration peak at 1735 cm^{-1} decreased in Co_3O_4@GO than pristine GO due to the interaction of Co_3O_4 NPs on the surface of GO sheets. The characteristic peaks of Co_3O_4 and GO turn into vanished or moved in the Co_3O_4@GO due to interaction of the between Co_3O_4 and GO sheets.

The XPS scrutiny was carried out to check the proportion and valence state of the elements in the Co_3O_4@GO nanocomposite. In the survey scanC, Co, and O were presented (Fig. 2A). The datawas confirm thatformation of Co_3O_4@GO. The magnified spectra of C1s (Fig. 2B) shows a higher intensity peak at 285.3 eV due to C=C/C-C bond and two comparatively lower intensity peaks at 286.7 eV, and 289.4 eV due to C-O, and O=C-O bond respectively[36,37]. The Co 2p spectrum exhibits Co $2p_{3/2}$ and Co $2p_{1/2}$, suggest the two spin-orbit doubles characteristic of Co^{2+} and Co^{3+}. Also, two shake-ups (satellites) peaks present in the Co 2p spectrum (Fig. 2C)[38]. The O1s XPS spectrum shows (Fig. 2D), the peak at 532.85 eV, which corresponds to the lattice oxygen present in the $Co_3O_4$and GO[39] which results further confirmed that the successful formation of the composite.

Morphological characterization of Co_3O_4@GO

The morphological view of Co_3O_4@GO was analyzed by FE-SEM and HR-TEM and shown in Fig. 3. From the FE-SEM (Fig. A and B) and TEM image (Fig. 3C) of the Co_3O_4, it can be observed that the Co_3O_4 NPs arranged in a regular hexagonal shape with the average diameter of the single Co_3O_4NP was calculated to be 90-100 nm. (Fig. 3D) shows an FE-SEM image of GO. It was detected that GO has a typical smooth and thin sheet. After the introduction of Co_3O_4 NPs on GO surface, the GO sheet is consistently enclosed with Co_3O_4NPs resulting in the formation of Co_3O_4@GO composite, clearly shows in the FE-SEM and TEM images (Fig. 3E and F). Higher magnification of TEM image exposes detail morphology of the Co_3O_4@GO composite (Fig. 3G).

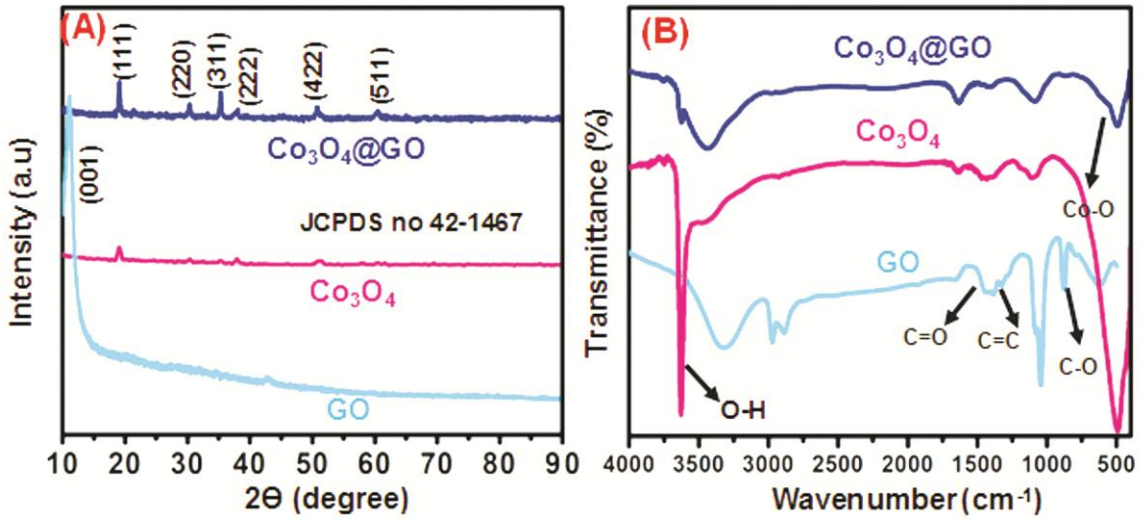

Fig. 1 — (A) XRD pattern, (B) The FT-IR spectrum of Co_3O_4 @GO nanocomposite

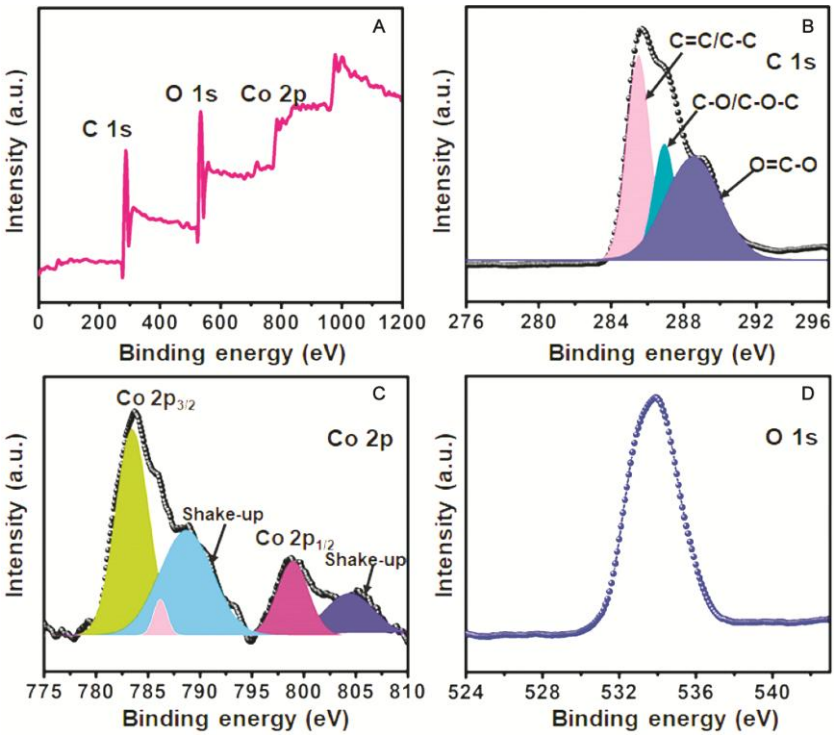

Fig. 2 — (A) XPS survey spectrum of Co_3O_4@GO, (B) high-resolution spectrum of C 1s, (C) Co 2p (D) O 1s of the Co_3O_4@GO.

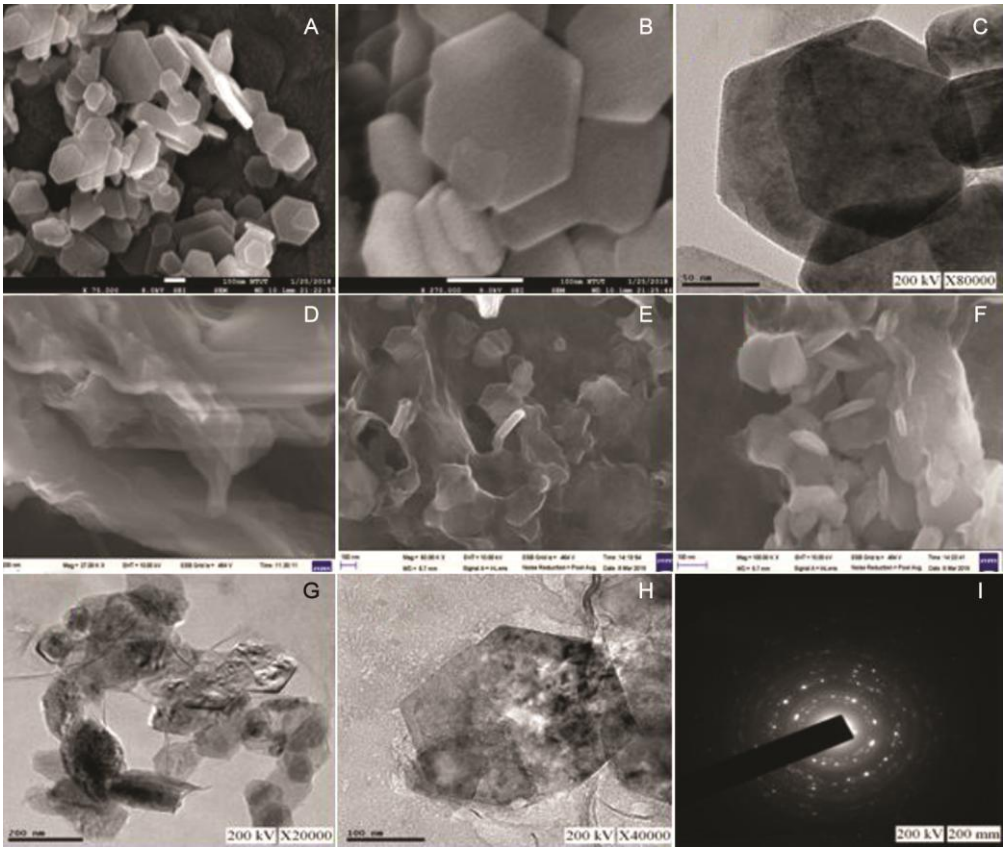

Fig. 3 — (A and B) ─ FE-SEM images; (C) HR-TEM image of the Co_3O_4; (D) FE-SEM image of the GO sheets; (E and F) FE-SEM images; (G and H) HR-TEM images and SAED pattern of the Co_3O_4@GO.

In which ultrathin layers of GO covered with the Co_3O_4Nps. Fig. 3H displays the SAED pattern of Co_3O_4@GO, which is in good accordance with the XRD pattern of Co_3O_4@GO. Also, EDX and elemental mappings analysis (Fig. 4A-D) prove the occurrence of C, O, and Co in Co_3O_4@GO.

Electrochemical behavior of the electrodes

The electrical conductivity of the bare GCE, GO/GCES, Co_3O_4/GCE and Co_3O_4@GO/GCE were examined using the EIS technique in presence of 0.1 M KCl with 0.005 M of $[Fe(CN)_6]^{-3/-4}$ solution and shown in Fig. 5A. The Nyquist plots in the frequency range of 100 kHz to 10 MHz are fitted by the Randles circuit model as shown in inset Fig. 5A. The Z_w, R_s, $R_{ct,}$ and C_{dl} are such as Warburg impedance, electrolyte solution resistance, charge-transfer resistance, and double layer capacitance, respectively[40]. For the bare GCE, the Rct value was calculated to be 81 Ω cm^2.After modified with GO the electrochemical impedance slightly dropped to 52 Ω cm^2. The Co_3O_4@GO/GCE showed a smaller Rct value of 8 Ω cm^2 than that of Co_3O_4/GCE (8 Ω cm^2). The smaller R_{ct} value was a consequence of the high-speed electron transfer process between the electrolyte and electrolyte, thus suggesting higher electrical conductivity of Co_3O_4@GO/GCE.

The electrochemical response of 100 µM FA at various electrode such as bare GCE, GO/GCE, Co_3O_4/GCE and Co_3O_4@GO/GCE (d) was investigated by cyclic voltammetry in 0.1M PB (*p*H 7.0) at scan rate 50 mV s^{-1} (Fig. 5B).It could be seen that the bare electrode does not show any signal for FA, which illustrates that the bare electrode has notendencyto activate FA. The Co_3O_4/GCE exhibits small broad oxidation peak with the potential of 0.83 V and GO/GCE exhibit noticeable oxidation peak of FA at 0.82 V. The Co_3O_4@GO/GCE exhibits sharp and well-defined oxidation peak at + 0.79. The oxidation peak potential was shifted to negative direction and the ipa of FA was enhanced than other electrodes due to the substrate of GO present transfer in between the Co_3O_4 NPs accelerate the electron enhance the electrocatalytic activity of Co_3O_4@GO towards FA.

Fig. 5C shows the CV curves of Co_3O_4@GO/GCE at various concentrations of FA (50–350 µM) in 0.1 M PB (pH 7.0) at a scan rate of 0.05 V s^{-1}. The ipa progressively enlarged with growing the concentration of FA from 50 to 350 µM. Besides, the results in Fig. 5D established worthy linearity between the ipa and the FA concentration with linear regression and coefficient of ipa= 0.115[FA]/(µM) +2.07 and 0.997 respectively.

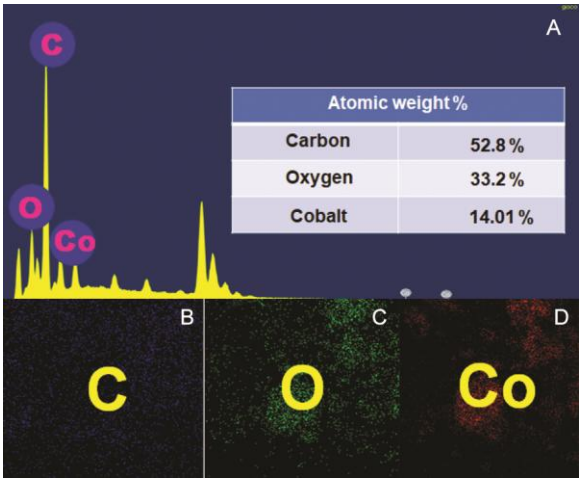

Fig. 4 — (A) EDX spectrum of Co_3O_4@GO. Insets: Quantitative analyses. (B-D) Mapping images of Co_3O_4@GO

Effect of Scan rate and *p*H on oxidation of FA at Co_3O_4@GOelectrode

The effect of scan rate at the Co_3O_4@GO/GCE towards an oxidation of FA was studied at increased scan rates from 0.02 to 0.2 V s^{-1} in 100µM of FA with 0.1 M PB (*p*H 7.0). Fig. 6A shows the peak current of FA increased with an increase in scan rate from 0.02 to 0.2 V s^{-1}. The ipa shifted towards the more positive sides while increase the scan rates, indicated that the Co_3O_4@GO/GCE has good electron transportation

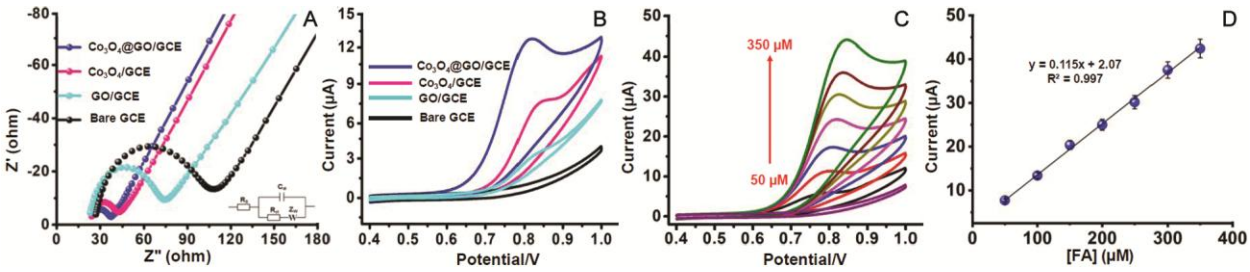

Fig. 5 — (A) EIS of bare GCE, GO/GCE, Co_3O_4/GCE and Co_3O_4@GO/GCE; (B) The CVs curves of bare GCE, GO/GCE, Co_3O_4/GCE and Co_3O_4@GO/GCE in PB (pH 7.0) containing 100 µM of FA at scan rate of 50 mV S^{-1}; (C) The CVs curves of various concentration of FA from 50 µM – 350 µM at Co_3O_4@GO/GCE and (D) the plot of current vs FA concentration.

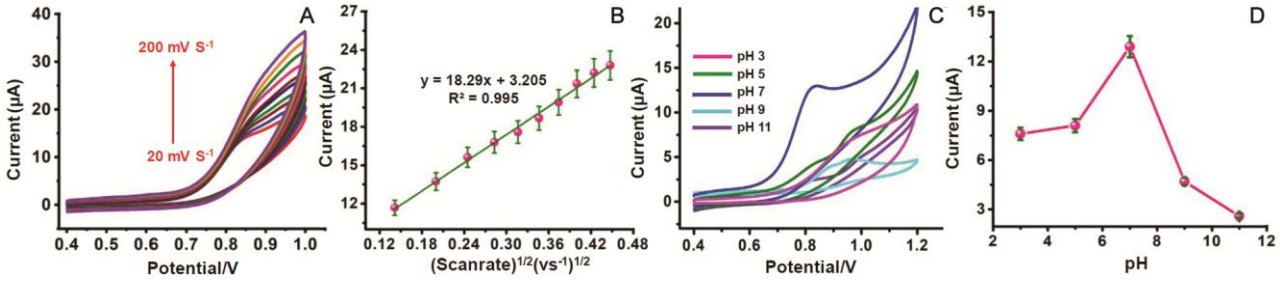

Fig.6 — (A) CVs for the oxidation 100 µM of FA on Co_3O_4@GO at different scan rates (20-200 mVs^{-1}) in 0.1 M PB (*p*H 7.0); (B) The plot of I_{pa} vs. square root of scan rate; (C) Effect of different *p*H on the 100 µM concentration of FA at Co_3O_4@GO in 0.1 M PB (*p*H 7.0) and (D) The plot of I_{pa} vs. *p*H.

and reaction kinetics. Besides, Fig. 6B shows excellent linearity between the ipa and the square root of scan rate with regression and coefficient of ipa= $18.29\upsilon^{1/2}(Vs^{-1})^{1/2}+3.205(R^2 = 0.995)$. These results presented that the reaction kinetics of Co_3O_4@GO/ GCE were thoroughly occurred by the diffusion controlled process.

The effect of the *p*H range of the buffer (pH 3.0–11.0) on the response of 100 µMof FA in the PB at Co_3O_4@GO was examined by CV (Fig. 6C). The correlation of *p*H to the oxidation peak current (I_{pa}) and was plotted and displayed in Fig. 6D. The higher $I_{pa}$was observed for *p*H 7 than that of other *p*H. Thus, *p*H 7.0 was chosen as the appropriateelectrolyte for the electrochemical sensing of FA at Co_3O_4@GO electrode.

The amperometric response of FA at Co_3O_4@GO/GCE

The amperometric (i-t) analysis was carried out to analyze the sensitivity and concentration dependency of the Co_3O_4@GO/GCE towards FA detection**.** Fig. 7A shows the amperometric (i-t) response of Co_3O_4@GO/GCE with the increasing concentration of the FA (0.1–4000 µM) 0.1 M PB (pH 7.0). The ipa was gradually increased with the increasing concentration of the FA. From the corresponding calibration plot presented in Fig. 7B, it was exhibited that the linear dependency between the ipaand the concentration of FA. The regression equation could be expressed as ipa [FA]=0.992 (µM)+29.70 and the coefficient (R^2) of 0.985. The limit of detection (LOD) was obtained to be 0.024 µM µM using the equation of LOD = 3 S/q and the sensitivity was calculated as 47.23 $\mu A\mu M^{-1}$ cm^{-2}. Where 'q' represents the slope value (0.992µA μM^{-1}) from the ipavs concentration of FA, and 'S' represents the standard deviation (STD) acquired from the three measurements of the blank signal (0.012µA).

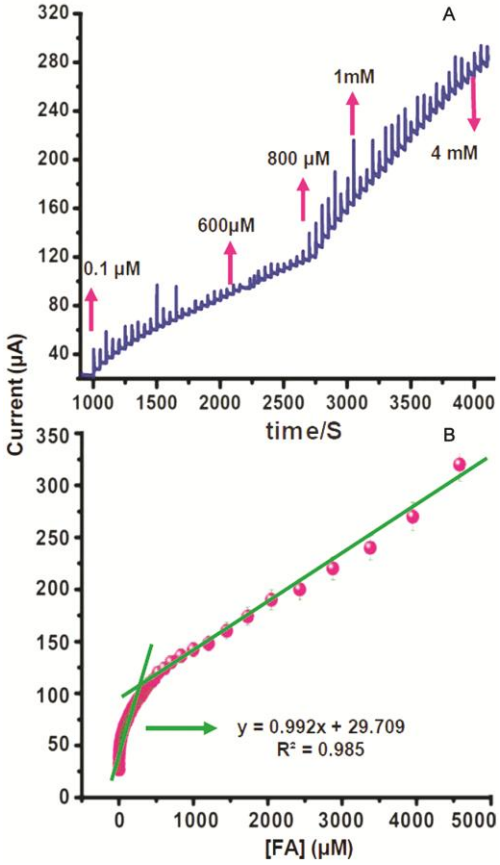

Fig. 7 — (A) Amperometric response ofCo_3O_4@GO/GCE at the concentration of FA from 0.1 to 4000 µM in PB (pH 7.0). and (B) Linear plot of current response (µA) versus concentration of FA (µM).

Real sample analysis

To investigate the accuracy of the Co_3O_4@GO/GCE for the FA sensing, Co_3O_4@GO/ GCE was further examined the real-time detection of FA in a biological sample of human urine sample. The urine samples were taken from the healthier volunteer and urine sample was prepared according to the literature[41]. First, human urine sample was diluted

Table 1 — Determination of FA in urineat Co_3O_4@GO modified electrode.

Samples	Added (μM)	Found (μM)	Recovery (%)	*RSD (%)
	0	0	-	0
Human urine	5	4.76	95.2	4.72
	10	9.58	95.8	3.52
	15	14.2	94.6	3.27

* Related standard deviation (RSD) of 3 independent experiments

with PB (1:10) and analyzed by the amperometric (i-t) instrument and it was found that the absence of FA in the real sample. Then the known concentration of FA was mixed to the real samples. The amperometric (i-t) analysis was performed by the standard addition method and the obtained recovery values are presented in Table 1 with acceptable results. The real-sample analysis of FA is successful and makes it conceivable for the real-time monitoring of FA without any notable influence from the interferences. diluted (1:10) with PBS (pH 7.4), and then appropriateamounts were transferred to the electrochemical cell and each species determined using the GNPs-Naf/SPE and DPV

Conclusion

In this work, we have synthesized Co_3O_4@GO composite and demonstrated it as superior catalytic performance for the detection of FA. The XRD, FTIR, XPS, FESEM, and HRTEM clearly showed the formation of the Co_3O_4@GO, and their electrochemical performances were studied by various electrochemical techniques. More considerably, the detection limit of the Co_3O_4@GO composite towards FA detection was found to be 0.024 μM with a wide linear range of 0.1 μM–4 mM and higher sensitivity of 47.23 $\mu A \mu M^{-1}$ cm^{-2}. The outcomes obtained from the recovery and competitive experiments ensure the applicability of the advanced method for the selective detection of FA under the co-existence of interfering specious. Thus, the strong advantages including high sensitivity, and excellent selectivity of the developed method provide important activities towards the real-time sensing of FA in all biological samples.

Acknowledgements

The authors gratefully acknowledge the financial support of the Ministry of Science and Technology, Taiwan through contract no. 107-2113-M413 027-005 MY3.

Competing interests

The author(s) declare no competing interests.

References

1 Wang Y, Yang M, Ren Y & Fan J, *Anal Chim Acta*, 1040 (2018) 136.
2 Murugan E, Santhoshkumar S, Govindaraju S & Palanichamy M, *Spectrochim Acta Part A*, 246 (2021) 119036.
3 Ratnayake S, Sandaruwan C, Mantilaka M, De Silva N, Dahanayake D, Wanninayake U, Bandara W, Santhoshkumar S, Murugan E & Amaratunga G, *J Ind Eng Chem*, Please tell me volume number (2020) Please tell me pages number.
4 Zhang H, Tian W, Zhou L, Sun H, Tade M & Wang S, *Appl Catal* B, 223 (2018) 2.
5 Sun Y, Jiang J, Liu Y, Wu S & Zou J, *Appl Surf Sci*, 430 (2018) 362.
6 Zou J, Wu S, Liu Y, Sun Y, Cao Y, Hsu J P, Wee A T S & Jiang J, *Carbon*, 130 (2018) 652.
7 Shao H, Zhao X, Wang Y, Mao R, Wang Y, Qiao M, Zhao S & Zhu Y, *Appl Catal B*, 218 (2017) 810.
8 Ratnayake S, Mantilaka M, Sandaruwan C, Dahanayake D, Murugan E, Kumar S, Amaratunga G & de Silva K N, *Appl Catal A*, 570 (2019) 23.
9 Zhang H, Tian W, Guo X , Zhou L , Sun H , Tadé M O & Wang S, *ACS Appl Mater Interf*, 8 (2016) 35203.
10 Wang M, Shen M, Zhang L, Tian J, Jin X, Zhou Y & Shi J, *Carbon*, 120 (2017) 23.
11 Xia P, Zhu B, Cheng B, Yu J & Xu J, *ACS Sust Chem Eng*, 6 (2017) 965.
12 Murugan E, Kumar S S, Reshna K & Govindaraju S, *J Mater Sci*, 54 (2019) 5294.
13 Kogularasu S, Govindasamy M, Chen S M, Akilarasan M & Mani V, *Sens Actuators B*, 253 (2017) 773.
14 Murugan E, Jebaranjitham J N & Usha A, *Appl Nanosci*, 2 (2012) 211.
15 Murugan E & Shanmugam P, *Bull Mater Sci*, 38 (2015) 629.
16 Murugan E, Santhosh Kumar S & Raman A, *AMP*, 3 (2018) 112.
17 Liu Y, Jiang J, Sun Y, Wu S, Cao Y, Gong W & Zou J, *RSC Adv*, 7 (2017) 36015.
18 Kong L, Ren Z, Zheng N, Du S, Wu J, Tang J & Fu H, *Nano Res*, 8 (2015) 469.
19 Gupta R, Boruah B, Modak J M & Madras G, *J Photochem Photobiol A*, Please tell me Volume number (2018) Please tell me pages number.
20 Chang X, Zhai X, Sun S, Gu D, Dong L, Yin Y & Zhu Y, *Nanotechnol*, 28 (2017) 135705.
21 Murugan E, Geetha Rani D, Srinivasan K & Muthumary J, *Expert Opin Drug Deliv*, 10 (2013) 1319.
22 Barkaoui S, Haddaoui M, Dhaouadi H, Raouafi N & Touati F, *J Solid State Chem*, 228 (2015) 226.
23 Sun S, Zhao X, Yang M, Wu L, Wen Z & Shen X, *Sci Rep*, 6 (2016) 19564.
24 Leng X, Wei S, Jiang Z, Lian J, Wang G & Jiang Q, *Sci Rep*, 5 (2015) 16629.
25 Sun H, Ang H M, Tadé M O & Wang S, *J Mater Chem A*, 1 (2013) 14427.
26 Zhao W, Zhou X, Kim I J & Kim S, *Nanoscale*, 9 (2017) 940-946.
27 Dai E, Xu J, Qiu J, Liu S, Chen P & Liu Y, *Sci Rep*, 7 (2017) 12588.
28 Bergmann A, Martinez-Moreno E, Teschner D, Chernev P, Gliech M, De Araújo J F, Reier T, Dau H & Strasser P, *Nat Commun*, 6 (2015) 8625.

29 Shi R, Chen G, Ma W, Zhang D, Qiu G & Liu X, *Dalton Trans*, 41 (2012) 5981.
30 Liu J, Wang J, Zhang B, Ruan Y, Wan H, Ji X, Xu K, Zha D, Miao L & Jiang J, *J Mater Chem A*, 6 (2018) 2067
31 Zhou X, Chen F, Cao F, Shen W, Liu J & Xu X, *Mater Lett*, 180 (2016) 175.
32 Mariyappan V, Keerthi M & Chen S M, *J Agric Food Chem*, 69 (2021) 2679.
33 Wang S, Wang R, Chang J, Hu N & Xu C, *Sci Rep*, 8 (2018) 1.
34 Zhang H, Wang X, Li N, Xia J, Meng Q, Ding J & Lu J, *RSC Adv*, 8 (2018) 34241.
35 Xu H, Hai Z, Diwu J, Zhang Q, Gao L, Cui D, Zang J, Liu J & Xue C, *J Nanomater*, Please tell me volume number 2015 (2015) Please tell me pages number.
36 Mutharani B, Keerthi M, Chen S M, Ranganathan P, Chen T W, Lee S Y & Chang W H, *ACS Appl Mater Interf*, 12 (2019) 4980.
37 Keerthi M, Mutharani B, Chen S M & Ranganathan P, *Microchim Acta*, 186 (2019) 1.
38 Ganesamurthi J, Keerthi M, Chen S M & Shanmugam R, *Ecotoxicol Environ Saf*, 189 (2020) 110035.
39 Dai X, Dai Y, Lu J, Pu L, Wang W, Jin J, Ma F & Tie N, *Ionics*, 26 (2020) 2501.
40 Mariyappan V, Keerthi M, Chen S M & Boopathy G, *J Electrochem Soc*, 167 (2020) 117506.
41 Krampa F D, Aniweh Y, Kanyong P & Awandare G A, *Arabian J Chem*, 13 (2020) 3218.